

## Plasticity of multiscale nanofilamentary Cu/Nb composite wires during *in situ* neutron diffraction: Codeformation and size effect

L. Thilly,<sup>a)</sup> P. O. Renault, and V. Vidal

Laboratoire de Métallurgie Physique, University of Poitiers, 86962 Futuroscope, France

F. Lecouturier

Laboratoire National des Champs Magnétiques Pulsés, UPS-INSA-CNRS, 31432 Toulouse, France

S. Van Petegem, U. Stuhr, and H. Van Swygenhoven

Paul Scherrer Institute, CH-5232 Villigen-PSI, Switzerland

(Received 11 January 2006; accepted 23 March 2006; published online 9 May 2006)

*In situ* neutron diffraction was performed on Cu/Nb nanocomposite wires composed of a multiscale Cu matrix embedding Nb nanofilaments with a diameter of 267 nm and spacing of 45 nm. The evolution of elastic strains and peak profiles versus applied stress evidenced the codeformation behavior with different elastic-plastic regimes: the Cu matrix exhibit size effect in the finest channels while the Nb nanowhiskers remain elastic up to the macroscopic failure, with a strong load transfer from the Cu matrix onto the Nb filaments. The measured yield stress in the finest Cu channels is in agreement with calculations based on a single dislocation regime. © 2006 American Institute of Physics. [DOI: 10.1063/1.2202720]

Multifunctional materials combining strength with functionality can be optimized by the design of multiple phase microstructures spanning multiple length scales from nanometers to micrometers. Materials for the winding of resistive coils producing nondestructive magnetic fields over 80 T are an example of such challenge: wires with both very high strength and high electrical conductivity are required.<sup>1</sup> In this context, nanofilamentary copper/niobium (Cu/Nb) conductors were processed via severe plastic deformation: they are composed of a conducting multiscale Cu matrix embedding reinforcing Nb nanofilaments and exhibit an ultimate tensile strength (UTS) of up to 2 GPa at 77 K for a total section of 5 mm<sup>2</sup> and filaments of 25 nm in diameter.<sup>2,3</sup> The effect of microstructure refinement on mechanical properties was studied using *in situ* deformation in a transmission electron microscope (TEM).<sup>4</sup> A single dislocation regime was observed in the Cu matrix confined at the nanometer scale, a mechanism that has also been reported for nanolayered composites.<sup>5,6</sup> Therefore, the associated strengthening was suggested to be modeled by an Orowan-type size dependence of the yield stress, as done for nanostructured multilayers:<sup>7-9</sup>  $\sigma_{y-Orowan} = (\alpha\mu/d)\ln(d/b)$ , where  $\alpha$  is a constant depending on the dislocation character and the Taylor factor,  $\mu$  the shear modulus,  $d$  the microstructure dimension, and  $b$  the length of Burgers vector. For the Nb filaments a whisker-type behavior was observed that is described by an exponential dependence of the yield stress:  $\sigma_{y-whisker}$  (Nb)  $\propto \exp(-d_{Nb})$ , approaching the theoretical shear strength for very small filaments diameter  $d_{Nb}$ . The macroscopic yield stress of Cu/Nb nanocomposite wires has then been modeled using a modified rule of mixture (mROM) that takes into account the strengthening induced by size reduction in each phase:<sup>4</sup>  $\sigma_{y-mROM}(Cu/Nb) = X_{Cu}\sigma_{y-ROM}(Cu) + X_{Cu-fine}\sigma_{y-Orowan}(Cu) + X_{Nb}\sigma_{y-whisker}(Nb)$ , where  $X_{Cu}$  and  $X_{Nb}$  are, respectively, the Cu and Nb volume fractions,  $\sigma_{y-ROM}(Cu)$  is the yield stress of severely cold worked Cu

matrix ( $\approx 350$ – $400$  MPa), and  $X_{Cu-fine}$  is the volume fraction of fine Cu regions where the single dislocation mechanism occurs (for the Orowan stress,  $\alpha=0.573$ ,  $\mu=42.5$  GPa, and  $b=0.256$  nm were used). The mROM values were found to be in good agreement with experimental mechanical properties.

Here, to justify the use of the Orowan-type and whisker-type laws for the nanofilamentary composite wires and to separate the contribution of each phase to their macroscopic yield stress, *in situ* neutron diffraction experiments are performed on bulk Cu/Nb wires. The experiments are conducted at the Swiss spallation neutron source SINQ (Paul Scherrer Institut, Villigen, Switzerland)<sup>10</sup> using the time-of-flight diffractometer with multiple pulse overlap (POLDI), a concept that is described elsewhere.<sup>11,12</sup>

*In situ* tensile tests are performed in two configurations, neutrons scattering at crystallographic planes parallel and perpendicular to the tensile axis, giving, respectively, transverse and axial strains in the Cu and Nb components. The evolution of the elastic strain for the different crystallographic lattice plane families versus the applied stress reveals the codeformation behavior of the Cu/Nb nanocomposite wire, while the study of the major Cu diffraction peak profiles reveals evidences of a size-dependent strengthening of the multiscale Cu matrix.

The tested Cu/Nb samples were processed via a series of hot-extrusion, cold-drawing, and bundling stages that are repeated four times to obtain the structures containing 55<sup>4</sup> Nb identical fibers.<sup>2,3</sup> The resulting Cu matrix is an assembly of multiscale channels, as shown in Fig. 1. Nb filaments (with an average diameter of 267 nm for a total Nb volume fraction  $X_{Nb}=29.5\%$ ) are separated by the finest Cu-0 channels (with a thickness  $d_{Cu-0}=45$  nm and a volume fraction  $X_{Cu-0}=10.2\%$ ); groups of 55 Nb fibers are separated by Cu-1 channels (with a width  $d_{Cu-1}=149$  nm and  $X_{Cu-1}=7.8\%$ ), etc. Finally, the group of 55<sup>4</sup> Nb filaments is embedded in the external Cu jacket, Cu-4. The dimensions of Cu-2, Cu-3, and Cu-4 channels are, respectively,  $d_{Cu-2}=1.27$   $\mu\text{m}$ ,  $d_{Cu-3}$

<sup>a)</sup>Electronic mail: ludoric.thilly@univ.poitiers.fr

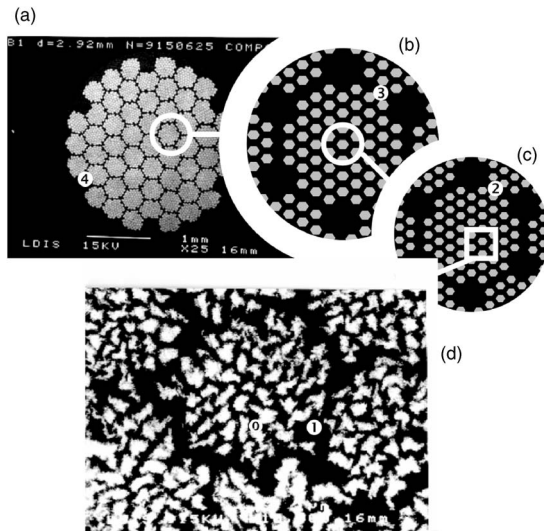


FIG. 1. Cross sections of the multiscale structure of the Cu/Nb conductors. [(a) and (d)] SEM micrographs; [(b) and (c)] sketches of intermediate scales. Nb filaments appear in white on highly magnified SEM micrograph (d) (conductor with  $d_{\text{Nb}}=524$  nm and  $d_{\text{Cu-0}}=89$  nm).

$=10.7$   $\mu\text{m}$ , and  $d_{\text{Cu-4}}=47$   $\mu\text{m}$  ( $X_{\text{Cu-2}}=11\%$ ,  $X_{\text{Cu-3}}=16\%$ , and  $X_{\text{Cu-4}}=25.5\%$ ). The tested sample has a total diameter of 1.49 mm and UTS of 1.1 GPa at 293 K. TEM investigations revealed that the cross section of the Nb filaments is composed of a few grains of about 100 nm diameter.<sup>13</sup> These grains are strongly elongated along the wire axis with a  $\langle 110 \rangle$  axial texture. The Cu-0 and Cu-1 channels contain only one grain in cross section; these grains are strongly elongated along the wire axis. The larger Cu- $i$  channels ( $i=2-4$ ) are composed of grains with diameters of 200–400 nm. X-ray diffraction evidenced a predominant macroscopic  $\langle 111 \rangle$  axial texture of the Cu matrix and a remnant  $\langle 200 \rangle$  component.<sup>2,13</sup>

The *in situ* tensile tests were performed at room temperature: more than ten stress states up to failure of the wire were recorded for both scattering configurations; neutron collection was started after stress relaxation of the sample. The position of several Cu and Nb diffraction peaks was followed versus the applied stress: for axial strain, only  $(220)_{\text{Nb}}$ ,  $(111)_{\text{Cu}}$ , and  $(222)_{\text{Cu}}$  diffraction peaks were intense enough for profile fitting, due to the presence of texture; for transverse strain, the  $(110)_{\text{Nb}}$ ,  $(211)_{\text{Nb}}$ , and  $(222)_{\text{Nb}}$  peaks and the  $(111)_{\text{Cu}}$ ,  $(200)_{\text{Cu}}$ ,  $(220)_{\text{Cu}}$ , and  $(311)_{\text{Cu}}$  peaks could be followed. Note that the  $(220)_{\text{Cu}}$  peak is the only reflection that is perpendicular to  $\langle 111 \rangle_{\text{Cu}}$ . All other reflections measured in transverse strain result from scattering in the non- $\langle 111 \rangle$  textured Cu zones. The strain was calculated using  $(d_{hkl} - d_{hkl}^0)/d_{hkl}^0$ , where  $d_{hkl}^0$  is the peak position in the pre-load state. Gaussian fits were used to determine peak positions, with errors smaller than  $10^{-4}$  Å. All  $(hkl)$  peaks were well fitted with a single Gaussian function, except the  $(220)_{\text{Cu}}$  peak in transverse configuration. Figure 2 shows, for neutrons scattering on planes parallel to the tensile axis, the  $(220)_{\text{Cu}}$  peak versus lattice spacing at two stress levels, pre-load ( $\sigma=31$  MPa) and  $\sigma=1062$  MPa. A strong peak asymmetry is observed at the high- $d_{hkl}$  side for small stress and at the low- $d_{hkl}$  side for high stress, the change occurring gradually during loading. This is more visible when plotting the difference between raw data and fit, i.e., the residuals displayed in inset of Fig. 2. This behavior is thought to be the evidence of different elastic-plastic responses of the multi-

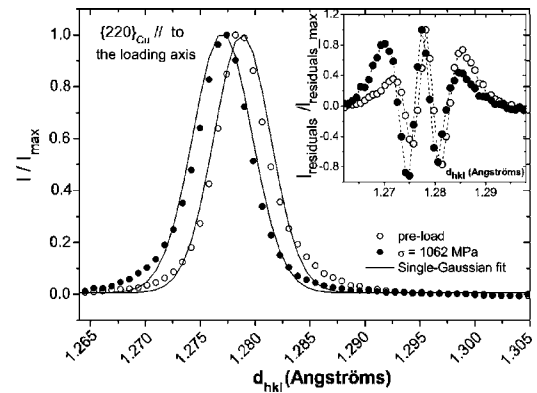


FIG. 2.  $(220)_{\text{Cu}}$  peak vs lattice spacing  $d_{hkl}$  at two stress levels, pre-load ( $\circ$ ) and  $\sigma=1062$  MPa ( $\bullet$ ), for neutrons scattering onto planes that are parallel to the tensile axis: symbols correspond to raw data and lines to single-Gaussian fits. Inset: residuals (i.e., difference between raw data and fit) vs  $d_{hkl}$ .

scale Cu matrix: 74.5% of the Cu matrix is composed of “bulk” Cu with grains in the 200–400 nm range (Cu-2–Cu-4 channels) whereas the Cu-0 and Cu-1 channels are composed of single nanograins of 45–150 nm. According to the results from *in situ* TEM experiments, “large-Cu channels” (Cu-2–Cu-4) behave as heavily cold worked bulk Cu, while the “fine-Cu channels” (Cu-0 and Cu-1) deform in a single elastic regime, which should be reflected in an enhanced elastic limit. Figure 2 also evidences the presence of residual stresses in the as-prepared sample: the Cu matrix is initially in axial compression ( $d_{220}^0 > a_{\text{Cu}}/8^{1/2}=1.276$ ); it is to be expected that these internal stresses are larger in the fine-Cu channels (being in direct contact with the Nb filaments) than in the large-Cu channels where internal dislocation rearrangements during the material’s synthesis are easier. In other words, the  $(220)_{\text{Cu}}$  diffraction peaks can be considered as being a superposition from two peaks: the first, from the fine-Cu channels with an initially high axial internal compressive stress, the second, coming from the large-Cu channels, with a lower axial internal compressive stress. Therefore, compared to the large-Cu peak (and for neutrons scattering onto  $\{hkl\}$  planes parallel to the tensile axis), the fine-Cu peak is (1) shifted towards high- $d_{hkl}$  values because of internal stress, (2) broadened because of smaller grain size, and (3) less intense because of a smaller volume fraction.

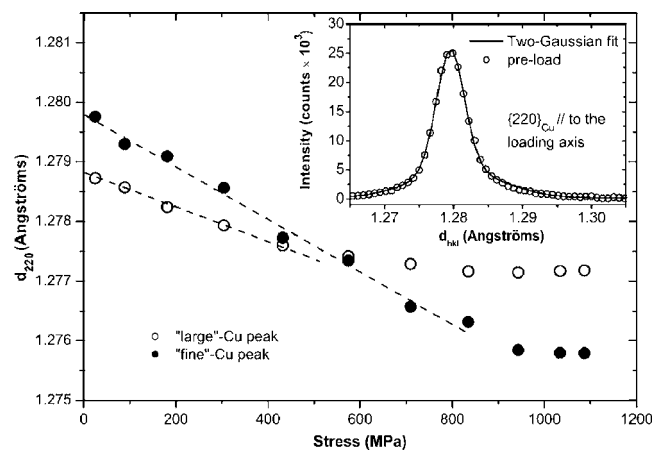


FIG. 3. Peaks positions from a two-Gaussian fit of the  $(220)_{\text{Cu}}$  peaks vs stress (neutrons scattering onto planes that are parallel to the tensile axis). Inset: corresponding  $(220)_{\text{Cu}}$  peak in the pre-load state.

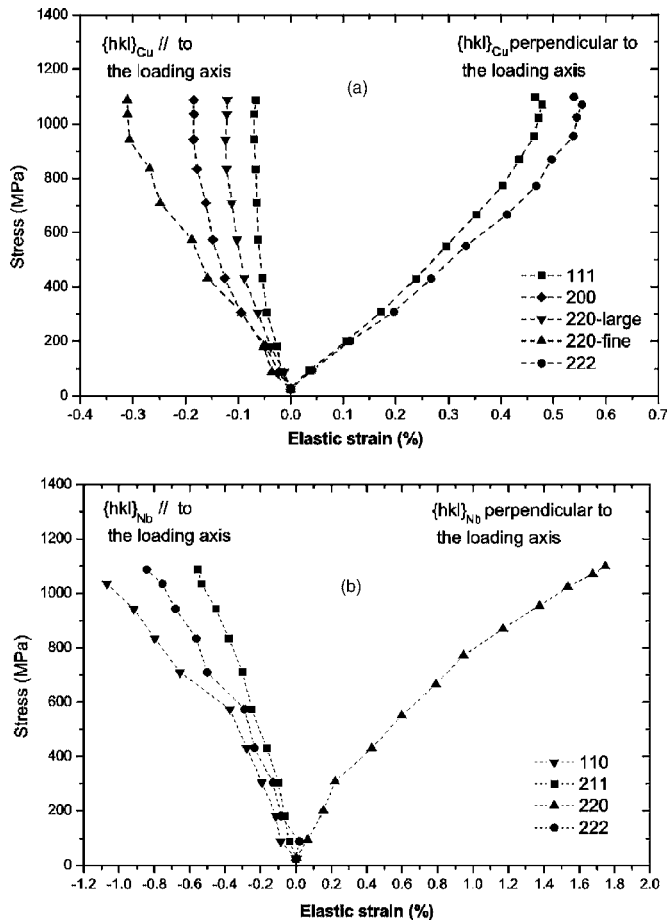


FIG. 4. Evolution of lattice elastic strain of dominant grain families in Cu (a) and Nb (b) for transverse and axial directions vs applied tensile stress. In the transverse strain configuration for Cu, the 311 curve has been omitted for clarity. Dashed lines are only to guide the eyes.

To separate the two contributions, the  $(220)_{\text{Cu}}$  peak profile was fitted using two Gaussian functions without fixing any parameters. For each stress state, two peaks were found with a ratio of full width at half maximum of 0.3 and a ratio of integrated intensity of 4, the latter corresponding approximately with the ratio of large to fine Cu channels volume fractions. These parameters were found to be similar at all stress states. Figure 3 shows the respective peak positions for the large-Cu and fine-Cu fits versus applied stress: the change in peak position of the large-Cu peak deviates from linearity at a stress of about 400 MPa, which is in agreement with the yield stress of highly cold worked Cu. However, deviation from linearity in the fine-Cu is only observed at 800–900 MPa. Applying the mROM to calculate the yield stress of the “fine” Cu, a value  $\sigma_{y\text{-mROM}}(\text{Cu-0}+\text{Cu-1}) = [X_{\text{Cu-0}}/(X_{\text{Cu-0}}+X_{\text{Cu-1}})] [\sigma_{y\text{-ROM}}(\text{Cu}) + \sigma_{y\text{-Orowan}}(\text{Cu-0})] + [X_{\text{Cu-1}}/(X_{\text{Cu-0}}+X_{\text{Cu-1}})] [\sigma_{y\text{-ROM}}(\text{Cu}) + \sigma_{y\text{-Orowan}}(\text{Cu-1})] = 893$  MPa is obtained, which is in good agreement with the observed deviation from linearity for fine-Cu channels (Fig. 3).

Figure 4 displays the evolution of the lattice transverse and axial elastic strain versus the applied stress for all dif-

fraction peaks followed for Cu [Fig. 4(a)] and Nb [Fig. 4(b)]. Figure 4(a) illustrates the elastic anisotropy of fcc Cu and the different elastic-plastic behaviors of the Cu channels: transverse strain measurements show that plasticity starts in the large Cu channels at a stress around 400 MPa (the 111, 200, 311, and 220 large curves), while the fine Cu channels yield around 900 MPa (the 220 fine curve). The axial strain derived from  $(111)_{\text{Cu}}$  and  $(222)_{\text{Cu}}$  peaks exhibits a behavior similar to the transverse strain of fine Cu channels derived from  $(220)_{\text{Cu}}$  peaks, with enhanced yield stress around 900 MPa; this indicates that the measured axial strains mainly originate from fine Cu channel grains. For the Nb phase [Fig. 4(b)], the elastic strain starts to increase faster above an applied stress of 600 MPa without leveling off. Such a behavior evidences load transfer from the plastifying Cu matrix into the Nb filaments, the latter remaining in the elastic regime up to sample fracture. This result confirms the whiskerlike behavior of Nb nanofilaments. The load transfer from Cu to Nb is also the footprint of the impenetrable character of Cu/Nb interfaces.

In summary, *in situ* deformation in a neutron beam allowed for detailed insight into the contributions of the different phases to the global deformation properties of a multi-scale nanoflamentary Cu/Nb wire: initially, with increasing stress, both Cu and Nb phases are deforming elastically until the largest Cu channels yield (around 400 MPa). At this stage, the finest Cu channels as well as the Nb nanofilaments are still deforming elastically, evidencing a size effect in the Cu matrix. The measured yield stress for the finest Cu channels is in agreement with an Orowan-type behavior with  $\sigma_{y\text{-Orowan}} \propto (1/d)\ln(d/b)$ , associated with the occurrence of a single dislocation regime. Once the whole Cu matrix is in the plastic regime, a strong load transfer is observed onto the Nb nanowhiskers that continue to deform elastically up to macroscopic fracture.

<sup>1</sup>K. Spencer, F. Lecouturier, L. Thilly, and J. D. Embury, *Adv. Eng. Mater.* **6**, 290 (2004).

<sup>2</sup>F. Dupouy, J. P. Peyrade, S. Askénazy, and D. Legat, *Physica B* **211**, 43 (1995).

<sup>3</sup>L. Thilly, F. Lecouturier, G. Coffe, J. P. Peyrade, and S. Askénazy, *IEEE Trans. Appl. Supercond.* **10**, 1269 (2000).

<sup>4</sup>L. Thilly, M. Véron, O. Ludwig, F. Lecouturier, J. P. Peyrade, and S. Askénazy, *Philos. Mag. A* **82**, 925 (2002).

<sup>5</sup>P. M. Anderson, T. Foecke, and P. M. Hazzledine, *MRS Bull.* **24-2**, 27 (1999).

<sup>6</sup>D. E. Kramer and T. Foecke, *Philos. Mag.* **82**, 3375 (2002).

<sup>7</sup>J. D. Embury and J. P. Hirth, *Acta Metall. Mater.* **42**, 2051 (1994).

<sup>8</sup>A. Misra, M. Verdier, Y. C. Lu, H. Kung, T. E. Mitchell, M. Nastasi, and J. D. Embury, *Scr. Mater.* **39**, 555 (1998).

<sup>9</sup>A. Misra, J. P. Hirth, and R. G. Hoagland, *Acta Mater.* **53**, 4817 (2005).

<sup>10</sup>This research project has been supported by the European Commission under the sixth Framework Programme through the Key Action: Strengthening the European Research Area, Research Infrastructures under Contract No. RII3-CT-2003-505925.

<sup>11</sup>U. Stuhr, *Nucl. Instrum. Methods Phys. Res. A* **545**, 319 (2005).

<sup>12</sup>U. Stuhr, H. Spitzer, J. Egger, A. Hofer, P. Rasmussen, D. Graf, A. Bollhalder, M. Schild, G. Bauer, and W. Wagner, *Nucl. Instrum. Methods Phys. Res. A* **545**, 330 (2005).

<sup>13</sup>F. Dupouy, E. Snoeck, M. J. Casanova, C. Roucau, J. P. Peyrade, and S. Askénazy, *Scr. Mater.* **34**, 1067 (1996).